Peridynamic-Based Modeling of Elastoplasticity and Fracture Dynamics

Haoping Wang[1] | **Xiaokun Wang** *[1] | **Yanrui Xu**[1,3] | **Yalan Zhang**[1] | **Chao Yao**[2] | **Yu Guo**[2] | **Xiaojuan Ban** *[1]

[1]School of Intelligence Science and Technology, University of Science and Technology Beijing, Beijing, China

[2]School of Computer and Communication Engineering, University of Science and Technology Beijing, Beijing, China

[3]University of Groningen, Netherlands

Correspondence
Corresponding author Xiaojuan Ban, University of Science andTechnology Beijing, Beijing, China.
Email: banxj@ustb.edu.cn
Corresponding author Xiaokun Wang, University of Science andTechnology Beijing, Beijing, China.
Email: wangxiaokun@ustb.edu.cn

This paper introduces a particle-based framework for simulating the behavior of elastoplastic materials and the formation of fractures, grounded in Peridynamic theory. Traditional approaches, such as the Finite Element Method (FEM) and Smoothed Particle Hydrodynamics (SPH), to modeling elastic materials have primarily relied on discretization techniques and continuous constitutive model. However, accurately capturing fracture and crack development in elastoplastic materials poses significant challenges for these conventional models. Our approach integrates a Peridynamic-based elastic model with a density constraint, enhancing stability and realism. We adopt the Von Mises yield criterion and a bond stretch criterion to simulate plastic deformation and fracture formation, respectively. The proposed method stabilizes the elastic model through a density-based position constraint, while plasticity is modeled using the Von Mises yield criterion within the bond of particle paris. Fracturing and the generation of fine fragments are facilitated by the fracture criterion and the application of complementarity operations to the inter-particle connections. Our experimental results demonstrate the efficacy of our framework in realistically depicting a wide range of material behaviors, including elasticity, plasticity, and fracturing, across various scenarios.

KEYWORDS
Peridynamic, Elastoplastic simulation, Fracture

1 | INTRODUCTION

In recent years, the physically based simulation of elastoplastic behavior and fracture animation has garnered significant interest, with applications extending to industrial simulations, human-computer interaction, medical surgery simulations, and the modeling of biological soft tissues. Among the traditional simulation methods, mesh-based approaches, particularly the Finite Element Method (FEM), have been widely utilized for elastoplastic simulations due to their established frameworks and accuracy. However, as the complexity of the models increases and issues such as mesh distortion, damage, and the need for mesh reconstruction arise, these methods often require the use of increasingly smaller time steps and finer mesh quality to maintain accurate results. This inherent limitation of mesh-based methods has led to the exploration and subsequent favoring of meshless methods in scenarios where dynamic topology changes and high degrees of deformation are prevalent.

Meshless methods, such as Smoothed Particle Hydrodynamics (SPH)[1] from fluid dynamics[1] to the simulation of elastic solids[2] has spurred great interest in meshless techniques due to their simplicity, accuracy in model sampling, and a unified framework for simulating interactions with fluids. These advantages have led to particle-based methods emerging as a novel approach in recent years. Notably, Müller *et al.*[3] introduce a mesh-free method for simulating stiff elastic and highly plastic objects, while Becker *et al.*[2] adapt the SPH method for elastic materials. Recent developments in particle-based SPH methods[4][5][6] have shown significant promise in simulating elastic and fluid phenomena.

However, these meshless methods rely on classical continuum theory and face challenges with non-uniform particle sampling and distribution, leading to decreased simulation effectiveness. Furthermore, they struggle with discontinuous boundary problems that are inherent to partial derivatives rather than differentials. Recent solutions to these issues involve creating virtual bonds
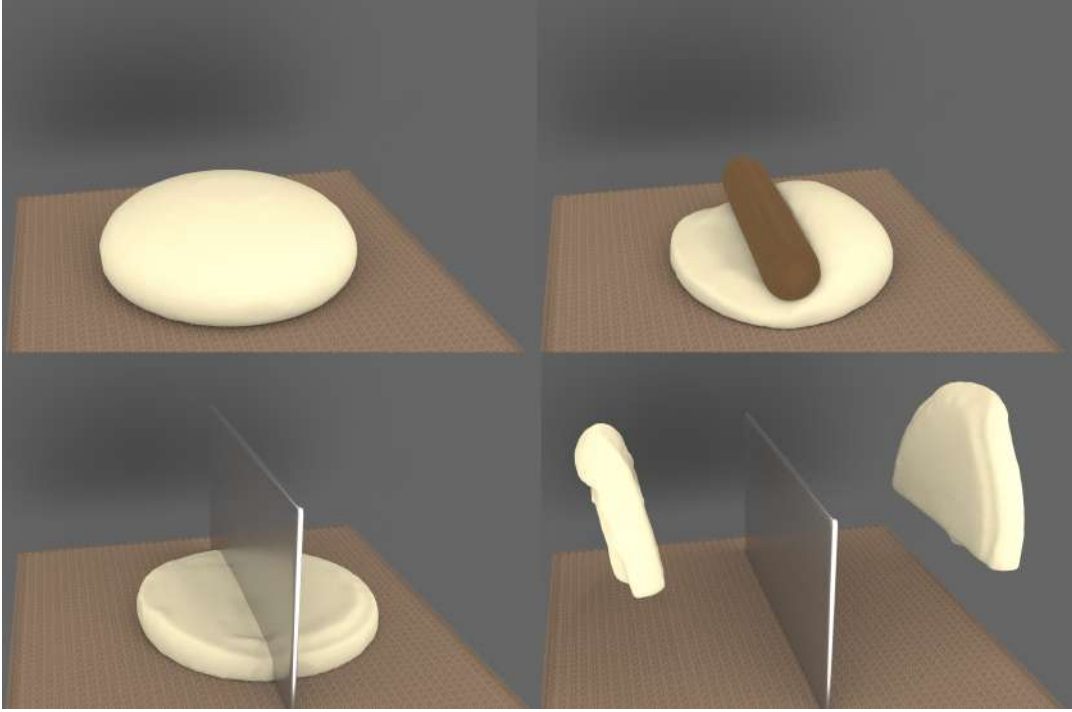
FIGURE 1 This paper presents a Peridynamic-based approach for elastoplastic and fracture simulation. This figure depicts the dough drops to the ground, flattened by a rolling pin and severed with a metal blade. Finally, we put the two distinct segments up for elastoplasticity.

in SPH[7] or employing mass-spring systems[8], which calculate interaction forces through connected bonds. While increasing the number of adjacent sampling particles can mitigate discontinuity issues, a comprehensive mathematical theory for these problems remains elusive in these methods.

Fortunately, Silling *et al.*[9] propose a robust meshless method capable of addressing discontinuous deformation and damage issues. Peridynamic, as introduced by them, offers an accurate simulation of thermoelastic and fracture damages. In originally bond-based Peridynamic, the Poisson's ratio in three-dimensional simulations is limited to 0.25. To overcome this limitation, state-based Peridynamic is developed, allowing simulations across a broader range of Poisson's ratios. Silling *et al.*[10][11] demonstrate the theoretical viability of simulating elastoplastic behavior and fracture damages using this approach. Building on this foundation, our work integrates Peridynamic into the simulation of elastic materials. Notable contributions in this domain include the work by Zhu *et al.*[12], who achieved elastoplastic and fracture effects by modifying the original Peridynamic formulations for elasticity and employing explicit numerical iteration methods. However, the small time steps required by their approach result in slow overall simulation speeds. He *et al.*[13][14] implement simulations of co-rotated elastoplastic viscous flows and hyperelastic energy model-based film simulations, respectively.

In this paper, we build upon the work of He[13] by introducing an elastoplastic solver based on a density constraint to ensure the stabilization of elastic simulations. Unlike previous methods that focused on viscous flow simulations using the Drucker-Prager criterion, our approach emphasizes the simulation of fracture effects in elastoplastic solids. We adopt the Von Mises yield criterion, introduce a complement operation, and achieve the simulation of fracture effects through the breakage of particle bonds.

2 | RELATED WORK

In computer graphics, the simulation of the elastoplastic solids has a long history. Both mesh and meshless methods have been continuously studied and proposed for better elastoplastic and fracture phenomenon. In this section, we will introduce some attractive developments in the field of elastoplastic and fracture simulation.

2.1 | Eulerian/Lagrangian Methods

2.1.1 | Eulerian methods

From the perspective of Eulerian method, Finite Element Method[15] is widely adopted approach to the simulation of deformable objects. Irving *et al.* present a efficient and robust FEM simulation of elastoplastic objects with large deformation. In addition, Bargteil *et al.*[16] introduce a plasticity model for large plastic deformations while preserving volume. Recently, Kugelstadt *et al.*[17] use operator splitting for deformation energy terms and present a improved implicit Euler method for more efficient and stable corotated FEM simulation.

In addition to simulating the behavior of elastoplastic materials, FEM has been extended to simulate the fracture of elastic and brittle materials. O'Brien *et al.*[18] first introduce FEM-based methods to simulate brittle and ductile fracture of solids. To address the remeshing near fracture and topological, the virtual node approach[19] is presented for the FEM mesh cutting without the need for high-resolution meshes. More recently, the Extended Finite Element Method (XFEM)[20] has been purposed with a remeshing-free method and a straightforward, low-cost geometrical cutting algorithm without additional geometry constructs. XFEM has provided a foundation for further research allowing for more efficient and robust simulations of material fracture.

2.1.2 | Lagrangian methods

As a typical Lagrangian method, Smoothed particle hydrodynamics is originally introduced in fluid simulation[1] and fluid-solid interaction[21]. Due to the advantages of Lagrangian method, physical properties could be calculated by approximating the values and their gradient at each particle using values from neighboring particles. Monaghanr *et al.*[22] firstly adapt SPH for simulating inelastic deformable objects. However, the standard SPH kernel gradient evaluation lacks first-order consistency, causing an inaccurate capture of rotational deformation. Becker *et al.*[2] captain the rotation with SPH variant of the shape matching method and propose corotational formulation with the linear Cauchy-Green tensor.

In recent years, more researches have been studied for SPH methods due to the unified framework of the fluid and solid interaction. Peer *et al.*[4] use a correction matrix ensure the first-order consistency of the kernel gradient and propose a implicit linear formulation allowing larger time steps. Subsequently, Kugelstadt *et al.*[5] introduce a penalty force for the zero-energy mode and purpose a new SPH operator splitting formulation with the volume conserving forces and stretching forces for the complex and multi-physics scenario. Inspired by the quasi-Newton methods[23] and Liu *et al.*[24] work, kee *et al.*[25] solve the optimization problem with the L-BFGS solver and support more complex hyperelastic models to further speed up the simulation process and details. Wang *et al.*[26] represent elastic objects with anisotropic properties to further mimic muscle contractions. Besides, Gissler *et al.*[27] propose an elastoplastic SPH approach with two implicit solvers and simulate various snow effects.

2.2 | Hybrid Methods

Combining the advantages of Lagrangian and Eulerian methods, Material Point Method (MPM) is a hybrid method which has been a popular approach to simulating a diverse range of materials in recent years. Stomakhin *et al.*[28] first introduce the MPM method into the snow simulation and incorporate the phase changes of snow. Subsequently, Jiang *et al.*[29] introduce a locally affine description of the velocity to enhance the transfer of information between particles and the grid.Hu *et al.*[30] replace the shape functions in the stress divergence term with Moving Meast Squares Method (MLS) and implement the double speed of simulation.Su *et al.*[31] purpose an adaptively updated Lagrangian MPM and recover MLS-MPM[30] by using a completely Eulerian formulation.

Besides, the fracture crack simulation has been studied by MPM methods in recent. Wolper *et al.*[32] introduce the continuum Damage Mechanics (CDM) into MPM with integrating a variational approach to crack evolution and an energy-based criterion for the isotropic fracture. Subsequently, Wolper *et al.*[33] extend the non-local CD-MPM with anisotropic damage mechanics for the anisotropic fracture of ductile materials. Fan *et al.*[34] has introduced the MPM into the brittle fracture simulation and achieve better visual effects.
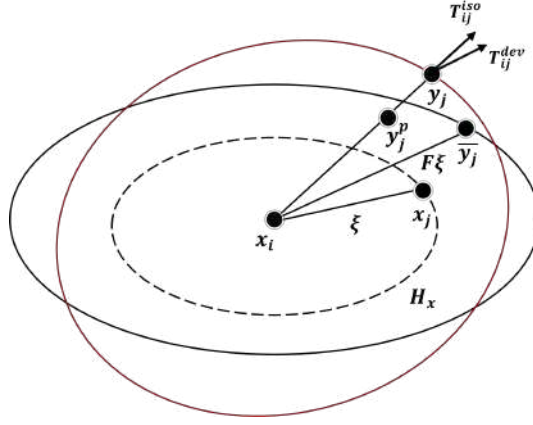
FIGURE 2 **Elastic state-based Peridynamic model**. The Dotted line represents the initial position state, the black line indicates the position state determined by the deformation gradient **F**, and the red line denotes the reference position state for deformation.

2.3 | Peridynamic

Peridyanmic is a non-local method to deal with the discontinues problem in engineering mechanics, and is first purposed by Silling *et al.*[9]. The origin form of Peridynamic is based on the bond[35], which limits the possion rate in 2-D as 0.33 and 3-D as 0.25, which are constant values. To overcome this problem, Silling *et al.*[10] subeuqently purpose a novel formulation named as state-based Peridynamic, which they introduce a new math tool referred as state to describe the mapping functions between connected particles. Besides, Silling *et al.*[36] has also proved that the theory of Peridynamic is infinitely close to the classical theory when the horizon is very small. Towards to the fracture, Silling *et al.*[37] gives the theory model of the fracture in Peridynamic. In computer graphics, Levine *et al.*[8] first introduce the Peridynamic model into the fracture simulation. Then, Zhu *et al.*[12] purposed the traditional Peridyanmic model after correction, they implement the elastic, plastic and fracture effects. He *et al.*[13][14] combine the classical constitutive models with Peridynamic and implement the elastoplastic model as well as hyperelastic membrane.

3 | PERIDYNAMIC THEORY

In this section, we briefly introduce the Peridynamic mathematical theory. In the Peridynamic theory[10], each particle have their own spherical neighborhood of distance δ. The δ is always called as horizon and the particles among its horizon are expressed as family $\mathcal{H}_x$. In state-based Peridynamic, let $\mathcal{L}_m$ become the set of all tensors of order m, we have a m-order state as a function:

$$\underline{\mathbf{A}}\langle\cdot\rangle : \mathcal{H}_x \to \mathcal{L}_m. \tag{1}$$

Thus, for any vector ξ representing the relative position of particles under the family $\mathcal{H}_x$, an order of state can be written as $\underline{\mathbf{A}}\langle\xi\rangle$. Given a kernel influence function $\underline{w} = W(\xi, \delta)$, for any two vector states under the family $\mathcal{H}_x$, $\underline{\mathbf{A}}\langle\xi\rangle$ and $\underline{\mathbf{B}}\langle\xi\rangle$, the calculation of second-order tensor $\mathbf{A}\langle\xi\rangle * \mathbf{B}\langle\xi\rangle$ can be defined by

$$\underline{\mathbf{A}} * \underline{\mathbf{B}} = \int_{\mathcal{H}_x} \underline{w}\langle\xi\rangle\underline{\mathbf{A}}\langle\xi\rangle \otimes \underline{\mathbf{B}}\langle\xi\rangle d\xi, \tag{2}$$

where $\otimes$ is the dyadic product. Thus, for a particle $\mathbf{x}_i$ and for any particle $\mathbf{x}_j$ in its horizon $\mathcal{H}_x$, we can define the rest reference position vector state $\underline{\mathbf{X}}$ and deformation reference position vector $\underline{\mathbf{Y}}$ as follows:

$$\begin{aligned} \underline{\mathbf{X}}\langle\xi\rangle &= \mathbf{x}_j - \mathbf{x}_i \\ \underline{\mathbf{Y}}\langle\xi\rangle &= \mathbf{y}_j - \mathbf{y}_i. \end{aligned} \tag{3}$$

Through all particles in the horizon $\mathcal{H}_x$, the shape tensor $\mathbf{K}$ of each particle can be calculated by the rest reference position vector in its horizon with:

$$\mathbf{K} = \underline{\mathbf{X}} * \underline{\mathbf{X}}. \tag{4}$$

Owning the shape tensor, we can define the deformation gradient $\mathbf{F}$ as a second order tensor as follows:

$$\mathbf{F} = (\underline{\mathbf{Y}} * \underline{\mathbf{X}})\mathbf{K}^{-1}. \tag{5}$$

In traditional elastic constitutive model, a common approach is using the deformation gradient to calculate the Cauchy stress tensor and the internal elastic force. In SPH Method, especially, the elastic force is by applying a kernel function to the neighboring particles to calculate the internal elastic potential energy and derivatives. Differently, the stated-based Peridynamic model uses asymmetry pair forces between two particles to describe the motion equation of the particle, their integral form is derived as:

$$\rho\ddot{\mathbf{u}} = \int_{\mathcal{H}_x} \left\{ \underline{\mathbf{T}}\langle\xi\rangle - \underline{\mathbf{T}}\langle-\xi\rangle \right\} dV_{\mathbf{x}} + \mathbf{b}, \tag{6}$$

where the ρ is the density of particle, $\ddot{\mathbf{u}}$ is the acceleration of the particle, $\underline{\mathbf{T}}$ is the force vector state between the particle and its neighbors, and b is the external force.

Algorithm 1 Elastoplasitc fracture Peridynamic solver

1: Input $\mathbf{y}^t$, $\mathbf{v}^t$, Ψ_0, β, α, s, dt
2: Advect($\mathbf{y}^t$, $\mathbf{v}^t$, dt)
3: Compute shape tensor K (Eqn. 24)
4: **while** position error>$error_{max}$ or iter<$iter_{max}$ **do**
5:      Compute deformation gradient F (Eqn. 25)
6:      Compute force density (Eqn. 11)
7:      Update position($\mathbf{y}^t$, $\Delta\mathbf{x}^t$) (Eqn. 12)
8:      Apply incompressible density constraint (Eqn. 14,15)
9:      Apply the Von Mises yield criterion (Eqn. 19)
10:     Search for the neighbour j
11:     Collision detection($\mathbf{y}^t$, $\Delta\mathbf{x}^t$)
12: **end while**
13: Update the fracture bond(Eqn. 22,23)

# 4 | PERIDYNAMIC BASED ELASTIC SIMULATION

In this paper, we purpose to construct the elastic energy for the constitutive model using the stated-based Periydnamics theory. In this section, we describe our discretization method of elastic simulation and incompressible density constraint.

4.1 | Co-rotated Elastic Energy Model

In the study of deformable objects, various constitutive models and energy functions [26] are utilized to capture the distinct properties of hyperelastic materials in elastic simulation. For the linear co-rotated constitutive model, the energy formula is commonly expressed as:

$$\Psi = \mu \|\mathbf{F} - \mathbf{R}\|^2 + \frac{\lambda}{2}(J - 1)^2, \tag{7}$$

where Ψ represents the potential energy, with μ and λ corresponding to the first and the second Lamé parameter, respectively. $\mathbf{R}$ denotes the rotation of the body, and J, the determinant of $\mathbf{F}$, is given as $J = det(\mathbf{F})$ to measure the change of unit volume. Similar to the the SPH method, we calculate the deformaiotn gradient by precomputing the shape tensor K and interpolating the kernel function across the neighboring particles with Eqn. (5).

(a)   (b)
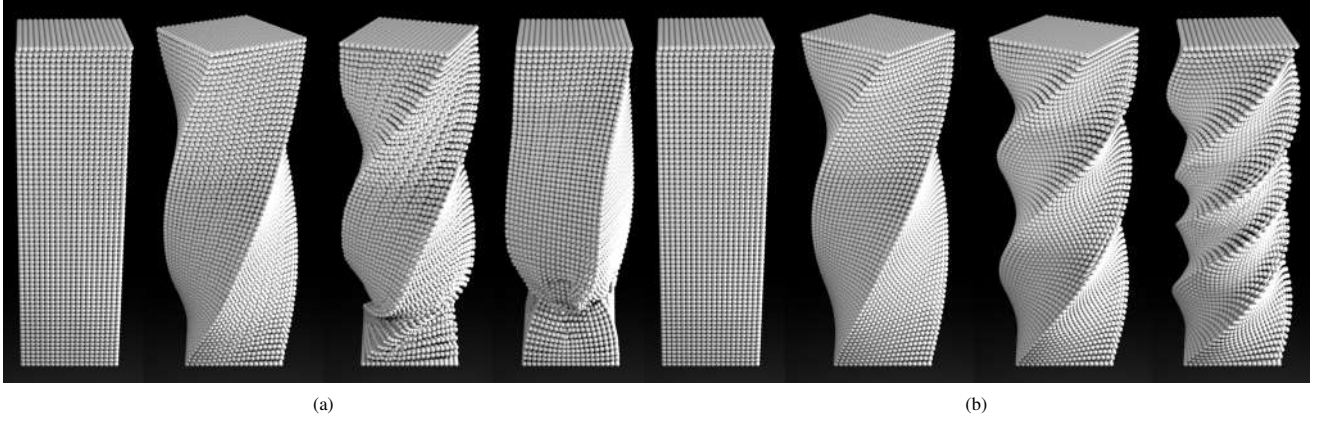
FIGURE 3   Elastic rotation tests with young's modulus of $E = 5 \times 10^4 \text{KPa}$ and a possion ratio of $\nu = 0.2$. (a) is Zhu *et al.* [12] method, and (b) is our method.

To apply the calculated potential energy into the discontinuous Peridynamic model, a significant challenge is to transfer the elastic energy of each particle to the bond of particle pairs. We first consider the right hand side of Eqn.(7) into two parts: the deviatoric part E^{dev} and isotropic part E^{iso} for our model, both of which acting as a bond energy between a particle pair. Then we can utilize the two part energy of each bond to get the energy model as:

$$\Psi = \sum_{H_x} \underline{w}\langle\xi\rangle \left(\mu E^{dev} + \frac{\lambda}{2} E^{iso} \right). \tag{8}$$

Since the deformation gradient $\mathbf{F}$ is consistent for all neighboring vertices in FEM method, we can also consider that in our Peridynamic system all neighboring particles share an identical deformation gradient value. Consequently, the reference position can therefore be obtained as $\overline{\mathbf{Y}} = \mathbf{F}\xi$. Consequently, E^{dev} and E^{iso} can be accordingly expressed as:

$$\begin{aligned} E^{\text{dev}} &= \left(\left|\overline{\mathbf{Y}}\right| / |\mathbf{X}| - 1 \right)^2 \\ E^{\text{iso}} &= \left(\left|\mathbf{Y}\right| / |\mathbf{X}| - 1 \right)^2. \end{aligned} \tag{9}$$

Subsequently, we can obtain the force density with $\frac{\partial E^{dev}}{\partial y_i}$ and $\frac{\partial E^{iso}}{\partial y_i}$ as:

$$\begin{aligned} \mathbf{T}^{dev} &= \frac{2\mu w}{|\mathbf{X}|^2}(\overline{\mathbf{Y}} - |\mathbf{X}| \operatorname{dir} \overline{\mathbf{Y}}) \\ \mathbf{T}^{iso} &= \frac{\lambda w}{|\mathbf{X}|^2}(\mathbf{Y} - |\mathbf{X}| \operatorname{dir} \mathbf{Y}), \end{aligned} \tag{10}$$

where dir $\mathbf{Y}$ contributes the normalized direction of Y. Here, $\mathbf{T}^{dev}$ is the force responsible for shear deformations, and $\mathbf{T}^{iso}$ is the force acting along the bond direction as shown in Fig 2. Due to the relatively small scale of the horizon, we assume that $|\overline{\mathbf{Y}}| - |\mathbf{X}| \approx |\mathbf{Y}| - |\mathbf{X}|$ and reformulate our elastic force density in Eqn. (10) as:

$$\begin{aligned} \mathbf{T}^{dev} &= \frac{2\mu w}{|\mathbf{X}|^2}(|\mathbf{Y}| - |\mathbf{X}|) \operatorname{dir} \overline{\mathbf{Y}} \\ \mathbf{T}^{iso} &= \frac{\lambda w}{|\mathbf{X}|^2}(|\mathbf{Y}| - |\mathbf{X}|) \operatorname{dir} \mathbf{Y}. \end{aligned} \tag{11}$$

Thus combining the implicit Euler integration and the Eqn. (6), we derive the differential form of the motion equation as:

$$\rho_i \mathbf{u} = h^2 \sum_j V_j (\mathbf{T}_{ij}^{dev}\langle\xi\rangle + \mathbf{T}_{ij}^{iso}\langle\xi\rangle - \mathbf{T}_{ji}^{dev}\langle-\xi\rangle - \mathbf{T}_{ji}^{iso}\langle-\xi\rangle), \tag{12}$$

where $\mathbf{u}$ is the relative displacement of particle, h is the time step, and V_j is the volume for the particle j under the within horizon $\mathcal{H}_x$.
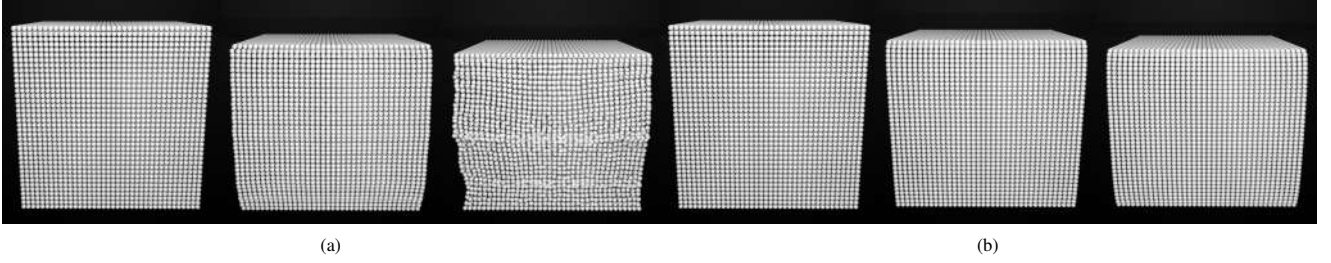
FIGURE 4 Elastic compression tests with young's modulus of $E = 2 \times 10^4$ KPa and a possion ratio of $\nu = 0.49$. (a) is Zhu *et al.* [12] method, and (b) is our method.

4.2 | Incompressible Density Constraint

To ensure the stability for the elastic model, we incorporate it with the density constraint C_i from Macklin *et al.* [38], with the form of :

$$C_i = \frac{\rho_i}{\rho_0} - 1, \tag{13}$$

where ρ_0 is the rest density, and ρ_i is the density calculated from the SPH method. The scaling factor for the position correction can therefore be expressed as:

$$\lambda_i = -\frac{C_i}{\sum_k \left| \nabla_{\mathbf{x}_k} C_i \right|^2 + \varepsilon}, \tag{14}$$

where ε is a user specified relaxation parameter that is constant over the simulation and the total corrected position update is:

$$\Delta \mathbf{x}_i = \frac{1}{\rho_0} \sum_j \left(\lambda_i + \lambda_j \right) \nabla W \left(\mathbf{x}_i - \mathbf{x}_j, h \right). \tag{15}$$

Above corrected positions can help the incompressibility and stability of our elastic approach. Moreover, the density constraint is affected significantly by the support radius. A larger radius will cause the expansion of the body, while a smaller radius may diminish the effect intended by our density constraint. As we test, a better parameter will be limited as 1.2-1.5 particle diameter throughout our experiment.

5 | PLASTICITY VON MISES MODEL

Plasticity and toughness are prevalent phenomena in materials science. In previous study, Muguercia *et al.* [39] introduce various approaches in computer graphics to plasticity and fracture damage. They decompose the total strain ε into elastic and plastic parts, adopting one yield point with Von Mises yield criterion to achieve plastic deformation. In theory of Peridynamic, Silling *et al.* [10] enable plasticity to be stored within the permanent deformation of bonds. And recently, Zhu *et al.* [12] successfully implement this mechanism into conventional peridynamic framework.

Different from the plastic model based on Drucker-Prager yield criterion [13], our plastic model utilizes the Von Mises yield criterion upon elastic Peridynamic model. Given the bond stretch ratio by $e = \frac{|\mathbf{y}_j - \mathbf{y}_i|}{|\mathbf{x}_j - \mathbf{x}_i|} - 1$, we decompose the bond stretch ratio $e = e_{ij} + e_{ij}^p$, where e_{ij} is the elastic component and e_{ij}^p is the plastic component. Considering that every active bond plastic deformation is only caused by the deviatoric part of elastic deformation, we decompose the elastic component of bond stretch into an isotropic part e^{iso} and a deviatoric part e^{dev}:

$$
\begin{aligned}
e^{iso} &= \int_{\mathcal{H}} \underline{w}\langle \xi \rangle e_{ij} d\xi \\
e^{dev} &= e_{ij} - e^{iso}.
\end{aligned}
\tag{16}
$$

Then we calculate the internal energy density of the bond with the deviatoric part of elastic deformation:

$$A_{dev} = \frac{(2\mu \underline{w} + \lambda \underline{w})}{\|\mathbf{x}_i - \mathbf{x}_j\|} e^{dev}. \tag{17}$$
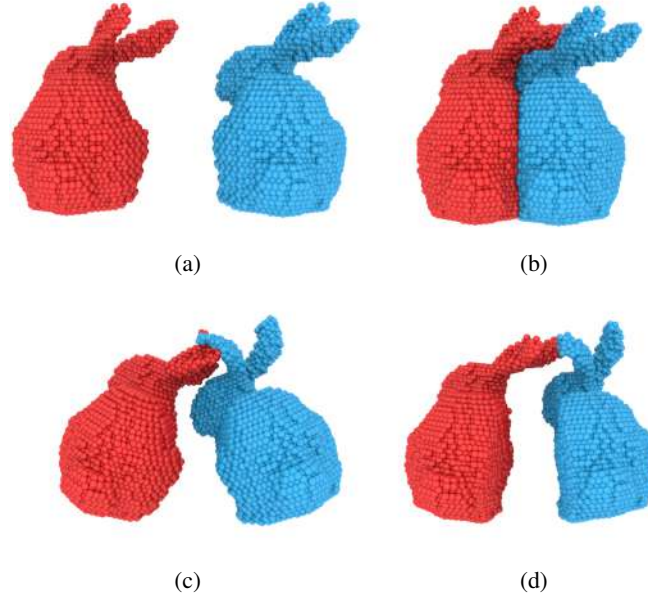
FIGURE 5 Two bunny collision with young's modulus of $E = 1 \times 10^5$ KPa and a possion ratio of $\nu = 0.25$. (a) is the initial configure of two bunnies, (b) is the collision between two bunnies, (c) and (d) are elastic and plastic configuration after collision, respectively

To determine whether plastic deformation occurs, we apply the Von Mises yield criterion and design a yield function as follows:

$$f(A_{dev}) = \frac{(A_{dev})^2}{2} - \Psi_0, \tag{18}$$

where the Ψ_0 represents the threshold value for the plastic criterion. When the internal energy density is rather than Ψ_0, the plastic variation has occurred. Otherwise, we determine the bond still keeps within the elastic domain. Thus, We calculate the deviant part of bond caused by the energy rather than the plastic criterion and get the plastic variation:

$$\triangle e^p = \frac{\|\mathbf{x}_i - \mathbf{x}_j\|}{\lambda}(A_{dev} - A_0 \, \text{sign}(A_{dev})), \tag{19}$$

where $A_0 = \sqrt{2\Psi_0}$ is the plastic yield point energy, $sign(.)$ is the sign function. While the plastic variation $\triangle e^p$ can not exceed e in the simulation, we add a control parameter β to make the plastic variation smaller when it is close to the deviatoric variation:

$$\triangle e^p = \kappa \triangle e^p$$
$$\kappa = e^\theta, \tag{20}$$

where $\theta = -\beta(\frac{\triangle e^p}{e_{dev} - \triangle e^p})^2$ is a quadratic function, β is the plastic control parameter and the κ is a exponential function. Furthermore, we update the plastic variation of every bond in elastoplastic objects.

6 | FRACTURE TREATMENT

In this section, we first introduce our fracture criterion to update the state between particles in 6.1. Then we represent the complement operation to avoid the mistake of deformation gradient under few neighboring particles in 6.2.

6.1 | Fracture Criterion

In traditional Peridynamic, fracture damage models are always solved by removing the bond between a particle and its neighbors. Owing to the differential applied in Peridynamic, this method sustains its accuracy when we incorporate traditional constitutive

(a) 1×10^{18} (b) 5×10^{18} (c) 1×10^{19}
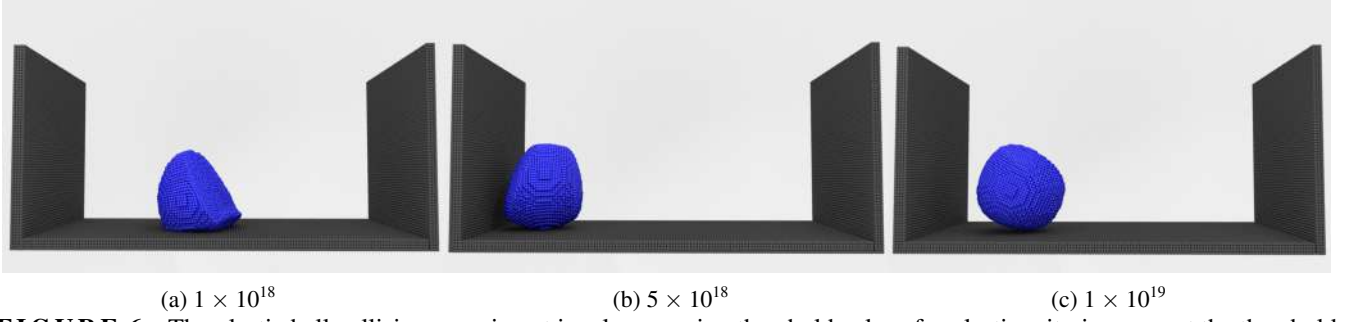
FIGURE 6   The plastic ball collision experiment involves varying threshold values for plastic criterion. we set the threshold values Ψ_0 as 1×10^{18} , 5×10^{18} ,1×10^{19} and β as 0.5 for (a), (b), (c).

models to state Peridynamic framework. Facing to the elastic brittle fracture, Silling *et al.*[35] has verified the feasibility through setting the fracture criterion. Thus, we rewrite the fracture criterion as:

$$s = e - e_{ij}^{p},, \tag{21}$$

where s is the maximum fracture criterion. When the actual stretch ratio of particle bond is greater than s, the bond between the particles will be removed. However, a significant issue is that the fracture parameter is difficult to control and causes more fragments. We therefore employed the method proposed by Zhu *et al.*[12] in which a refined fracture criterion is computed by incorporating with the weight function w and increasing the crack threshold with the material damaged:

$$s = (1 + \alpha\phi)\frac{(e - e_{ij}^{p})\mathbf{x}_{ij}}{\delta}, \tag{22}$$

where $\phi = 1 - \frac{n_i}{N_i}$ is the inactive ratio of the total connected bonds, α is the enhancement factor. Unfortunately, their method for traditional Peridynamic is not quite available in our fracture criterion, thus, we change the ϕ in our fracture criterion as:

$$\phi = 1 - (\frac{n_i}{N_i})^2, \tag{23}$$

where n_i is the inactive number of bonds and N_i is the active number of bonds. The quadratic form of this function makes the parameters to be better controlled to show the fracture and damage crack.

6.2 | Complement Operation

In our framework, fracture and cracking in elastoplastic materials break the bonds between particles, reducing the number of active bonds, which further cause the shape tensor not being positive definite and the error calculation of the deformation gradient. Drawing on the Kirchhoff–Love plate theory[40], which is used to analyze the mechanical behavior of slab structures and to simulate this cloth and membranes, we treat the particles with less bonds as slabs. Moreover, we introduce virtual particles to form a virtual slab. We first consider the particles i as the origin and construct virtual particles as $\mathbf{x}_i^*$ and rotation to establish our virtual slab. Then, we use the virtual slab to calculate the normal n_i. Subsequently, we construct the virtual normal particles, denoted as $\mathbf{x}_i^{\perp}$ with the thickness to represent the normals.

Therefore, we rewrite the shape tensor $\mathbf{K}$ in Eqn. (4) to:

$$\mathbf{K} = \sum_j \omega_{ij} \left(\mathbf{x}_j - \mathbf{x}_i\right) \left(\mathbf{x}_j - \mathbf{x}_i\right)^T + \sum_j \omega_{ij} \left(\mathbf{x}_j^* - \mathbf{x}_i\right) \left(\mathbf{x}_j^* - \mathbf{x}_i\right)^T + \left(\mathbf{x}_j^{\perp} - \mathbf{x}_i\right) \left(\mathbf{x}_j^{\perp} - \mathbf{x}_i\right)^T. \tag{24}$$

Similarly, $\mathbf{y}_j^*$ and $\mathbf{y}_j^{\perp}$ can be used to rewrite deformation gradient $\mathbf{F}$ as:

$$\mathbf{F} = \left(\sum_j \omega_{ij} \left(\mathbf{y}_j - \mathbf{y}_i\right) \left(\mathbf{x}_j - \mathbf{x}_i\right)^T + \sum_j \omega_{ij} \left(\mathbf{y}_j^* - \mathbf{y}_i\right) \left(\mathbf{x}_j^* - \mathbf{x}_i\right)^T + \left(\mathbf{y}_j^{\perp} - \mathbf{y}_i\right) \left(\mathbf{x}_j^{\perp} - \mathbf{x}_i\right)^T \right) \mathbf{K}^{-1}. \tag{25}$$

FIGURE 7 The back of the Armadillo is fixed while its limbs are gradually stretched and then completely torn off.

With this method, we can guarantee the shape tensor K to be positive definite and correct the deformation gradient $\mathbf{F}$ with Eqn. (25). When encountering single particle condition, our solution is to set their deformation gradient as the identity matrix because of the lack of the neighboring.

T A B L E 1 Simulation information for all examples

Example	particle num	Time step per frame	Max iter	Simulation time per frame
Elastic cuboid rotation	26.8k	1ms	5	8.6ms
Elastic cuboid compression	54.8k	1ms	5	23.1ms
Elastoplastic bunny	23.3k	2ms	5	21.7ms
Plastic ball	22.8k	2ms	5	18.6ms
Plastic wall fracture	30k	1ms	5	16.2ms
Cloth cut	87.8k	5ms	6	261.3ms
Armadilo fracture	195k	2ms	5	75.4ms
Dough compress and cut	230k	2ms	5	162.2ms

7 | EXPERIMENTS AND RESULTS

In this section, we present a series of experiments to validate the robustness and stability of our elastoplastic and fracture approach. we conduct our experiments using the Python and Taichi and rendering via Houdini. In order to better display the location of cracks in our experiments, we show the proportion of the unconnected bonds of the particles. As shown in Fig 8 and Fig 9, while the color of the particles is closer to red, indicating more unconnected bonds, which is also the generation of cracks, the color of the particles is closer to blue, indicating that no cracks are generated. Additionally, We provide a comprehensive demonstration of the algorithmic workflow in Algorithm 1 and the information for simulation performance in various experiments in Table 1. As demonstrated in Table1, our method ensures rapid simulation efficiency without incorporating plasticity and fracture. Upon adding plasticity and fracture components, larger simulation time is necessary to achieve better simulation results.

7.1 | Rotation and compression

We first design an experiment involving the compression and rotation of a fixed elastic cube and compare our method incorporating density constraint to the method by Zhu *et al.* [12]. Here, We establish the same angular and compression velocity in our experiment acting as the external force and verify the stability and accuracy of our elastic simulation. As shown in Fig 3 and Fig 4, Zhu *et al.* [12] method appears instability following the application of rotation and compression under special parameter conditions. On the contrary, our method can always maintain stable effect with our density constraint radius as 0.7δ throughout the simulation.

FIGURE 8 Collision between rigid ball and thin plastic wall.

7.2 | Elastoplastic bunny collision

We demonstrate the effectiveness of our elastoplastic model, with comparing two experiments involving the collision between bunnies. Because of the difference in plastic materials of the bunnies in two experiments, which one exhibits purely elasticity while the other exhibits both elasticity and plasticity, the two bunnies present different shapes after the collision. As illustrated in Fig 5, the elastic bunnies revert to its original state, while the bunnies with plasticity display both plastic deformation and volume compression after collision.

7.3 | Plastic ball simulation

This experiment depicts the plastic behavior with different threshold values of plastic criterion, aiming to observe the changes of different plastic states. Here, We impart an initial velocity to the ball and allow the plastic ball to collide with walls to test capacity for the plastic deformation. The simulation parameters set for the ball are Young's modulus of 6×10^5 KPa and the possion ratio of 0.25. As shown in Fig 6, with the decrease of plasticity threshold value, the range of plastic deformation changes become larger and the degree of changes become easier.

7.4 | Armadilo limbs tear

To verify the experimental results of fracture with multiple particles, we employ a armadilo model with particle sampling. In this experiment, the back of armadillo is secured in place while its limbs are progressively extended. As the extending increase, the limbs of armadilo are torn apart and the extended part will also recover to its original length over time as shown in Fig 7. The simulation parameters set for the armadilo model as Young's modulus of 5×10^4 KPa, the possion ratio of 0.2, the bond fracture criterion s with 0.2 and the fracture parameter α of 20.

7.5 | Plastic thin wall fracture

Fig 8 showcases the fracture and cracks occurring after the collision between the thin plastic wall and the ball to validate fracture effects in our elastoplastic framework. We design the ball to collide against a plastic thin wall at a constant velocity and the fracture and plastic deformation appears after the stability of the plastic wall. In this experiment, the simulation parameters set for the plastic wall are the Young's modulus of 7×10^5 KPa, the possion ratio of 0.25, the bond fracture criterion s with 0.06 and the fracture parameter α of 15.

7.6 | Cloth cut

The crack propagation of thin shell material under natural conditions can also show the validity and effectiveness of the fracture in our framework. Thus, We put a thin layer of cloth over the surface of a sphere, and then use the knife to cut a small cut in the top layer of the cloth. With the gravity exerting on the cloth, cracks and fracture generate in the cloth and the cloth falls to the
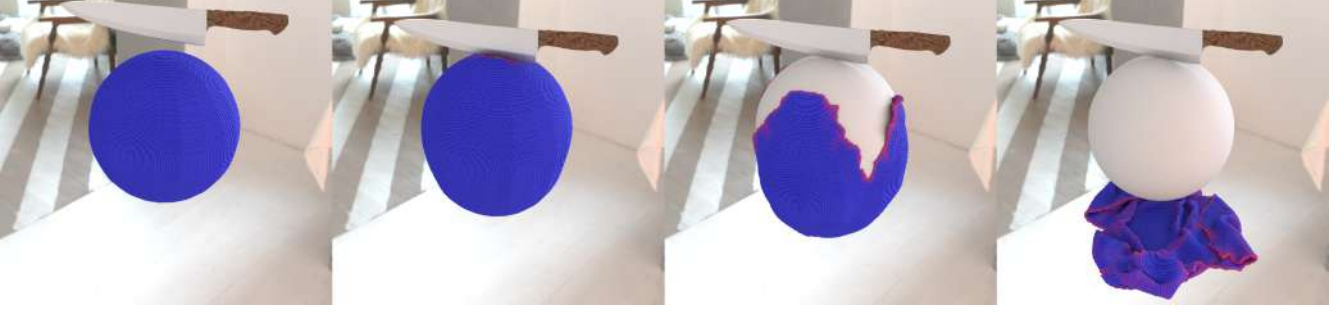
FIGURE 9 With the thin cloth over the surface of the sphere, we cut the top of cloth with knife and the thin cloth produces fractures and cracks with gravity.

ground, as shown in Fig 9. The simulation parameters set for the cloth model as Young's modulus off 3×10^4 KPa, the possion ratio of 0.3, the bond fracture criterion s with 0.1 and the fracture parameter α of 12.

7.7 | Compression and cutting of dough

This scenario in Fig 1 visualizes the simulation process that the dough dropping to the ground, compressed with a rolling pin and severed by a metal blade into two segments and finally two segments of dough are put into both sides, emulating the behavior of the interaction between elastoplastic materials and rigid bodies. The setup substantiates that the capability of our framework to accurately simulate both the elastoplastic behavior and the fractures of the material, providing a realistic scene of plastic dough changes. The simulation parameters in this experiment set as Young's modulus off 2×10^3 KPa, the possion ratio of 0.3, the threshold value Ψ_0 as 1×10^{18}, the bond fracture criterion s with 0.15 and the fracture parameter α of 10.

8 | CONCLUSION

In this paper, we present a particle-based peridynamic framework designed to simulate elastoplastic and fracture behaviors of different materials. Our approach transfers the co-rotated elastic energy of each particle to the bond of particle pairs based on peridynamic theory and incorporates an incompressible density constraint of specified support kernel radius within our elastic framework to enhance realism and stability. Then we employ the Von Mises yield criterion of different threshold values in our framework for various plasticity simulation and add a control parameter avoiding large plastic variation. Finally, we utilize bond fracture criterion and the complementarity method to address the stability issues arising from the lack of particles, thereby simulating fracture phenomena. This technique is efficient and stable under large elastic and plastic deformation as well as the scenario with generation of fracture and cracks.

However, our approach also restricts the types of elastoplastic material due to the lack of one-to-one theoretical basis of Peridynamic with the constitutive energy model in the traditional continuum methods. During the process of simulating plasticity, the formulation lacks energy conservation source and the extra energy caused by the plastic deformation will cause the loss of kinetic energy and velocity. Besides, the complementarity operation in fracture simulation will inadvertently introduce extra energy, making the control of parameters challenging.

In future work, we mainly concentrate on three key aspects of our framework. First, we aim to extend the constitutive model of elastic simulation to encompass more scenarios, integrating them with the concepts in Peridynamic to simulate various behaviors of elastic materials. Second, due to the issues of additional energy in elastoplasticity and fracture simulation, we propose to incorporate an energy correction term acting as a constraint to mitigate numerical errors and enhance stability. Lastly, the coupling with different phases of elastic material is an attractive topic in recent years. Grounded in the discontinuity principle of Peridynamic theory, we are keen to explore the coupling of discontinuous surfaces, representative of fractures, with fluid dynamics, delving into fluid-structure interactions within the Peridynamic theroy.

ACKNOWLEDGEMENTS

References

1. Becker M, Teschner M. Weakly compressible SPH for free surface flows. In: 2007:209–217.

2. Becker M, Ihmsen M, Teschner M. Corotated SPH for Deformable Solids.. *NPH.* 2009;9:27–34.

3. Müller M, Keiser R, Nealen A, Pauly M, Gross M, Alexa M. Point based animation of elastic, plastic and melting objects. In: 2004:141–151.

4. Peer A, Gissler C, Band S, Teschner M. An implicit SPH formulation for incompressible linearly elastic solids. In: . 37. Wiley Online Library. 2018:135–148.

5. Kugelstadt T, Bender J, Fernández-Fernández JA, Jeske SR, Löschner F, Longva A. Fast corotated elastic SPH solids with implicit zero-energy mode control. *Proceedings of the ACM on Computer Graphics and Interactive Techniques.* 2021;4(3):1–21.

6. Xiaokun Wang YX, Sinuo Liu BR, Ji˘r˘ı Kosinka ACT, Jiamin Wang CS, Jian Chang CL, Jian Jun Zhang XB. Physics-based fluid simulation in computer graphics: Survey, research trends, and challenges. *Computational Visual Media(CVM).* 2024. doi: doi.org/10.1007/s41095-023-0368-y

7. Islam MRI, Peng C. A Total Lagrangian SPH method for modelling damage and failure in solids. *International Journal of Mechanical Sciences.* 2019;157:498–511.

8. Levine JA, Bargteil AW, Corsi C, Tessendorf J, Geist R. A Peridynamic Perspective on Spring-Mass Fracture.. In: 2014:47–55.

9. Silling SA. Reformulation of elasticity theory for discontinuities and long-range forces. *Journal of the Mechanics and Physics of Solids.* 2000;48(1):175–209.

10. Silling SA, Epton M, Weckner O, Xu J, Askari E. Peridynamic states and constitutive modeling. *Journal of elasticity.* 2007;88:151–184.

11. Silling SA. Linearized theory of peridynamic states. *Journal of Elasticity.* 2010;99:85–111.

12. Chen W, Zhu F, Zhao J, Li S, Wang G. Peridynamics-Based Fracture Animation for Elastoplastic Solids. In: . 37. Wiley Online Library. 2018:112–124.

13. He X, Wang H, Wu E. Projective peridynamics for modeling versatile elastoplastic materials. *IEEE transactions on visualization and computer graphics.* 2017;24(9):2589–2599.

14. Lu Z, He X, Guo Y, Liu X, Wang H. Projective Peridynamic Modeling of Hyperelastic Membranes With Contact. *IEEE Transactions on Visualization and Computer Graphics.* 2023.

15. Sifakis E, Barbic J. FEM simulation of 3D deformable solids: a practitioner's guide to theory, discretization and model reduction. In: , , , 2012:1–50.

16. Bargteil AW, Wojtan C, Hodgins JK, Turk G. A finite element method for animating large viscoplastic flow. *ACM transactions on graphics (TOG).* 2007;26(3):16–es.

17. Kugelstadt T, Koschier D, Bender J. Fast corotated FEM using operator splitting. In: . 37. Wiley Online Library. 2018:149–160.

18. O'brien JF, Hodgins JK. Graphical modeling and animation of brittle fracture. In: 1999:137–146.

19. Molino N, Bao Z, Fedkiw R. A virtual node algorithm for changing mesh topology during simulation. *ACM Transactions on Graphics (TOG).* 2004;23(3):385–392.

20. Koschier D, Bender J, Thuerey N. Robust extended finite elements for complex cutting of deformables. *ACM Transactions on Graphics (TOG).* 2017;36(4):1–13.

21. Akinci N, Ihmsen M, Akinci G, Solenthaler B, Teschner M. Versatile rigid-fluid coupling for incompressible SPH. *ACM Transactions on Graphics (TOG).* 2012;31(4):1–8.

22. Monaghan JJ. Smoothed particle hydrodynamics. *Annual review of astronomy and astrophysics.* 1992;30(1):543–574.

23. Nocedal J, Wright SJ. *Numerical optimization.* Springer, 1999.

24. Liu T, Bouaziz S, Kavan L. Quasi-newton methods for real-time simulation of hyperelastic materials. *Acm Transactions on Graphics (TOG).* 2017;36(3):1–16.

25. Kee MH, Um K, Kang H, Han J. An Optimization-based SPH Solver for Simulation of Hyperelastic Solids. In: . 42. Wiley Online Library. 2023:225–233.

26. Wang T, Xu Y, Li R, Wang H, Xiong Y, Wang X. Simulating hyperelastic materials with anisotropic stiffness models in a particle-based framework. *Computers & Graphics.* 2023;116:437–447.

27. Gissler C, Henne A, Band S, Peer A, Teschner M. An implicit compressible SPH solver for snow simulation. *ACM Transactions on Graphics (TOG).* 2020;39(4):36–1.

28. Stomakhin A, Schroeder C, Chai L, Teran J, Selle A. A material point method for snow simulation. *ACM Transactions on Graphics (TOG).* 2013;32(4):1–10.

29. Jiang C, Schroeder C, Selle A, Teran J, Stomakhin A. The affine particle-in-cell method. *ACM Transactions on Graphics (TOG).* 2015;34(4):1–10.

30. Hu Y, Fang Y, Ge Z, et al. A moving least squares material point method with displacement discontinuity and two-way rigid body coupling. *ACM Transactions on Graphics (TOG).* 2018;37(4):1–14.

31. Su H, Xue T, Han C, Aanjaneya M. A-ULMPM: An Adaptively Updated Lagrangian Material Point Method for Efficient Physics Simulation without Numerical Fracture. In: . 41. Wiley Online Library. 2022:325–341.

32. Wolper J, Fang Y, Li M, Lu J, Gao M, Jiang C. CD-MPM: continuum damage material point methods for dynamic fracture animation. *ACM Transactions on Graphics (TOG).* 2019;38(4):1–15.

33. Joshuah W, Yunuo C, Minchen L, et al. Anisompm: Animating anisotropic damage mechanics. *ACM Transactions on Graphics (TOG).* 2020;39(4):37–1.

34. Fan L, Chitalu FM, Komura T. Simulating brittle fracture with material points. *ACM Transactions on Graphics (TOG).* 2022;41(5):1–20.

35. Silling SA, Askari E. A meshfree method based on the peridynamic model of solid mechanics. *Computers & structures.* 2005;83(17-18):1526–1535.

36. Silling SA, Lehoucq RB. Convergence of peridynamics to classical elasticity theory. *Journal of Elasticity.* 2008;93:13–37.

37. Silling SA, Askari A. Peridynamic model for fatigue cracking.. tech. rep., Sandia National Lab.(SNL-NM), Albuquerque, NM (United States); : 2014.

38. Macklin M, Müller M. Position based fluids. *ACM Transactions on Graphics (TOG).* 2013;32(4):1–12.

39. Muguercia L, Bosch C, Patow G. Fracture modeling in computer graphics. *Computers & graphics.* 2014;45:86–100.

40. Panc V. *Theories of elastic plates*. 2. Springer Science & Business Media, 1975.

AUTHOR BIOGRAPHY

Haoping Wang is a postgraduate student in Intelligent science and Technology, University of Science and Technology Beijing. He received an undergraduate Diploma in Computer Science and Technology from University of Science and Technology Beijing in 2022. His research area is computer graphics, specifically physics-based elastic solids simulation.

Xiaokun Wang is an associate professor in Intelligence Science and Technology, University of Science and Technology Beijing, China. He received a Ph.D. degree in Computer Science and Technology from the University of Science and Technology Beijing, in 2017. He is currently working at the National Centre for Computer Animation at Bournemouth University funded by the EU's Horizon 2020 Marie Curie Individual Fellowship. His research interests include computer graphics, virtual reality and human-computer interaction.

Yanrui Xu is a PhD student at Bernoulli Institute, University of Groningen and the School of Intelligence Science and Technology, University of Science and Technology Beijing. He received his Master's degree from the University of Science and Technology Beijing in 2020. His research interests include physical-based fluid simulation.

Yalan Zhang is a lecture at the School of Intelligence Science and Technology, University of Science and Technology Beijing. She received her Ph.D.degree in computer science and technology from the University of Science and Technology Beijing. Her research interests include computer graphics, intelligence simulation and 3D visualization.

Yu Guo received his B.S. degree in 2014 and Ph.D. degree in 2020 from University of Science and Technology Beijing, China. Now he is a lecturer in the School of Computer and Communication Engineering at University of Science and Technology Beijing, China. His main research interests include edge-cloud cooperation and embodied AI.

Chao Yao received the M.E. degree and Ph.D. degree from Beijing Jiaotong University (BJTU) in 2010 and 2016. From 2014 to 2015, he was a Visiting Ph.D. student at Swiss Federal Institute of Technology (EPFL). He is currently an Associate Professor with University of Science and Technology Beijing(USTB), researching video compression, computer vision and human-computer interaction.

Xiaojuan Ban is a professor at the School of Intelligence Science and Technology, University of Science and Technology Beijing. She is the leader of the Artificial Intelligence and 3D Visualization Group at University of Science and Technology Beijing, China. She received her Ph.D. degree in control theory and control engineering from the University of Science and Technology Beijing. Her research interests include computer graphics, artificial intelligence, human-computer interaction, big data analysis, and 3D visualization.